Structural Consequences of Carboxyamidation of Dermaseptin S3†

Deborah E. Shalev,‡ Amram Mor,‡ and Irina Kustanovich*,§

The Wolfson Centre for Applied Structural Biology and The Department of Biological Chemistry, The Silberman Institute of Life Sciences, The Hebrew University of Jerusalem, Safra Campus, Givat Ram, 91904 Jerusalem, Israel

Received December 6, 2001; Revised Manuscript Received March 18, 2002

ABSTRACT: Animal-derived antimicrobial peptides are gaining increasing interest for their role in the innate immune system and for their potential applications in the antimicrobial field. Defining the factors that affect potency and selectivity is presently a major challenge to their effective and safe use. Since amidating the C-terminal carboxyl is one of the means of enhancing antimicrobial activity, we report here our comparative study of the solution structures of the antimicrobial peptide dermaseptin S3 and its amidated analogue. Circular dichroism measurements suggested that the peptides are basically found in an α-helical structure. In contrast, NMR measurements revealed the complete absence of α-helical elements in S3 and a single four-residue helix in the amidated analogue. Whereas the native peptide was found to be flexible, containing a hydrogen-bonded turn and bends, the amidated analogue exhibited a defined α-helix at the C-terminal region, causing the latter to be significantly elongated and more structured. Hence, although the increased potency in amidated antimicrobial peptides can be attributed to the increased overall positive charge, in this case, amidation has had additional effects beyond modifying the net positive charge. It has induced and/or stabilized a helical conformation, causing the amidated dermaseptin to be more rigid and more extended than its nonamidated analogue. The possible implications on the mode of action are discussed herein.

Antimicrobial peptides are ubiquitous in nature. They have been shown to serve as the primary line of defense of both plants (*1*) and animals (*2*) and are effective against a range of bacterial and fungal pathogens (*3*−*5*). The precise mechanism of action of these peptides is not known, but they are believed to target the lipid component of cell membrane(s) and disrupt the membrane structure (*6*−*8*) possibly via the "barrel stave" mechanism (*9*−*11*) or the "carpet-like" mechanism (*12*−*14*). According to these models, the peptides induce cell permeabilization by inserting themselves and aggregate perpendicular or parallel to the membrane plane, respectively. Although the detailed molecular events that lead to cell lysis are not yet clear, such antimicrobial agents are attracting increasing interest for their potential uses against multidrug resistant pathogens given that their externally localized target and their receptor-independent mode of action could escape many of the mechanisms that lead to drug resistance. The factors known to affect cytolytic activity include the established correlation between the cationic charge of the peptides and their antimicrobial activity (*8*, *15*−*18*), showing that the first stage in the process includes an electrostatic attraction between the cationic peptide and the negatively charged headgroups of the membrane lipids (*8*). This step is corroborated by the correlation between increased positive charge on the peptide and membrane lytic activity (*19*−*21*). Knowing the precise atomic organization of the peptides could help in understanding the nature of the interaction with the membrane and eventually help in conceiving improved analogues.

Many antimicrobial peptides occur naturally in the carboxyamidated form. There are studies that show an increase in activity following amidation, and also a decrease in activity when the amide is removed (*2*). Amidation of dermaseptin S3, for instance, resulted in a 10-fold increased potency against pathogenic microorganisms (*22*). These facts indicate the importance of this modification to the activity of the peptides. The cause for this often dramatic change in activity remains to be addressed properly, although it has been ascribed to the increase in the total positive charge of the peptide, the change in overall dipole moment, and/or the reduced susceptibility to degradation by carboxypeptidases (*23*−*25*).

Dermaseptin S3 is a member of a large family of antimicrobial peptides isolated from the skin of South American tree frogs (*26*, *27*). These 24−34-amino acid peptides show cytolytic activity against a broad spectrum of pathogenic microorganisms (e.g., bacteria, protozoa, yeast, and filamentous fungi). Circular dichroism (CD)[1] experiments suggested that the structure of these polycationic peptides is medium-dependent, being unstructured in polar solvents but readily forming amphipathic α-helices in apolar

† This research was supported by the DA'AT consortium, a Magnet project administered by the Office of the Chief Scientist at the Ministry of Industry and Trade, Israel.

* To whom correspondence should be addressed: The Department of Biological Chemistry, The Silberman Institute of Life Sciences, The Hebrew University of Jerusalem, Safra Campus, Givat Ram, 91904 Jerusalem, Israel. Telephone: (+972 2) 6585575. Fax: (+972 2) 6585573. E-mail: irinak@macbeth.ls.huji.ac.il.

‡ The Wolfson Centre for Applied Structural Biology.

§ The Department of Biological Chemistry.

[1] Abbreviations: NMR, nuclear magnetic resonance; CD, circular dichroism; RBC, red blood cells; HPLC, high-pressure liquid chromatography; TFE, trifluoroethanol; NOESY, nuclear Overhauser effect spectroscopy; TOCSY, total correlation spectroscopy; rmsd, root-mean-square deviation; SD, standard deviation; MIC, minimal inhibitory concentration.

10.1021/bi016013m CCC: $22.00
Published on Web 05/17/2002

Table 1: Primary Structures of Dermaseptins S3, Its Amidated Derivative S3a, and S4

Peptide[a]	Number of residues	
S3	30	$_{NH2}$ALWKNMLKGIGKLAGKAALGAVKKLVGAES$_{COOH}$
S3a	30	$_{NH2}$----------$_{CONH2}$
S4	28	$_{NH2}$----TL--KVL-A-A----K--//----NA$_{COOH}$

[a] Sequences are given in one-letter code. A dash (−) represents an identical residue. Gaps (/) were introduced into S4 to maximize alignment with S3.

solvents (*28*). The antimicrobial action of these peptides was shown to be mediated by specific interactions of the amphipathic α-helix moiety with the plasma membrane phospholipids leading to cell permeabilization (*6*−*8*, *29*; reviewed in ref *30*). Dermaseptin S3 is a potent killer of nongrowing and slow-growing bacteria, suggesting a potential use in the eradication of bacteria in a dormant state and/or subject to low oxygen tension (*31*). In contrast, most conventional bactericidal or bacteristatic antibiotics are not effective against dormant bacteria, or those under conditions of oxygen deficiency. Toward possible application as food preservatives, a dermaseptin S3 derivative was demonstrated to effectively kill spoilage yeast (*32*).

Despite their high level of homology, the dermaseptin family members differ markedly in their biological properties. Dermaseptins S3 and S4 (sequences in Table 1), for instance, display different spectra of cytolytic activity in their toxicity toward red blood cells (RBC). Dermaseptin S3 was shown to selectively kill the intraerythrocytic parasite in *Plasmodium falciparum*-infected RBC without harming the host cell. Dermaseptin S4, on the other hand, displayed high antimalarial activity but poor selectivity (*33*). Investigations into the molecular basis for this selective cytotoxicity indicated that both dermaseptins were highly lipophilic, as demonstrated by their excellent ability to bind to and permeabilize phosphatidylserine/phosphatidylcholine vesicles (*29*). Dermaseptin S4, however, was found to be aggregated in contrast to S3. These differences in activity and in aggregation states suggested that there could be a structural basis for the variance in peptide properties. To verify such a possibility, we recently undertook an examination of the solution structures of both peptides.

Here, we report the results of our investigation of the structures of S3 and its amidated analogue, S3a, under the same experimental conditions that were used for S4 (*33*). Native dermaseptin S3 exhibited conformational flexibility, whereas its carboxyamidated analogue exhibited a defined α-helix loop in the C-terminal region. This finding suggests that carboxyamidation may cause additional molecular modifications beyond the increase in positive charge.

MATERIALS AND METHODS

Peptide Preparation. Dermaseptin S3 and its amidated analogue were synthesized by the solid phase method, applying the Fmoc active ester chemistry basically as described previously (*28*). HMP-resin (4-hydroxymethylphenoxymethyl-copolystyrene-1% divinylbenzene resin, Wang resin) and MBHA-resin (4-methylbenzhydrylamine, Novabiochem) were used to obtain free carboxyl and amidated peptide, respectively. After removal of the Fmoc group from the N-terminal amino acid, the peptides were cleaved from the resin with an 85:5:5:5 mixture of trifluoroacetic acid, *p*-cresol, H_2O, and thioanisole (10 mg of resin-bound peptide in 1 mL of mixture). The trifluoroacetic acid was then evaporated, and the peptide was precipitated with ether followed by washing with ether (six times). The crude peptides were extracted from the resin with 30% acetonitrile in water and purified to chromatographic homogeneity in the range of 98 to >99% by reverse-phase HPLC (Alliance-Waters). HPLC runs were performed on a semipreparative C4 column using a linear gradient of acetonitrile in water (1%/min), with both solvents containing 0.1% trifluoroacetic acid. The purified peptides were subjected to amino acid analysis and electrospray mass spectrometry to confirm their composition. Peptides were stocked as a lyophilized powder at −20 °C. Prior to being analyzed, fresh solutions were prepared in a 20% trifluoroethanol (TFE) solution in water.

Circular Dichroism Measurements. Circular dichroism spectra in millidegrees were measured with an AVIV model 62A DS spectrometer (Aviv Associates, Lakewood, NJ) using a 0.020 cm rectangular QS Hellma cuvette at 25 °C (controlled by thermoelectric Peltier elements with an accuracy of 0.1 °C). CD spectra were taken for peptide samples in water at first; then trifluoroethanol was added to a final concentration of 20% (v/v) TFE/water, and the spectra were recorded. CD data represent average values from three separate recordings.

NMR-Derived Three-Dimensional Structures. Samples of dermaseptin S3 and S3a were analyzed in a 1.4 mM solution of 20% (v/v) trifluoroethanol-d_3 in water. The effective pH of the samples ranged between 3 and 4. NMR data were acquired at a ^{1}H frequency of 600.13 MHz on an Avance Bruker DMX NMR spectrometer. The carrier frequency was set on the water signal whose chemical shift was 4.66 ppm relative to an external reference of trimethylsilylpropionate salt (Cambridge Isotope Laboratories) at 0 ppm. A range of temperatures between 280 and 310 K was examined to determine optimal conditions for the NMR measurements that balance minimal amide proton exchange with maximal spectrum spread. Structural data were acquired at 310 K. All experiments were carried out in the phase-sensitive mode (TPPI or States−TPPI) with 4K complex data points in t_2 and 512 t_1 increments, and were recorded with a spectral width of 12 ppm. A 90° pulse width of 7.5 μs was used, and the water signal was suppressed by cw irradiation during the relaxation delay of 1.5 s and the mixing times of the NOESY experiments. TOCSY experiments, carried out using the MLEV-17 pulse sequence for the spin lock (*34*), were used to identify the spin systems; NOESY (*35*, *36*) experiments were conducted with mixing times between 60 and 300 ms to obtain the maximal NOE buildup that showed no significant contribution from spin diffusion. Structural information was taken from NOESY spectra with mixing times of 150 ms. Zero filling was added to the indirect dimension, and the free induction decays were apodized in both dimensions with a shifted squared-sine window function to enhance spectral resolution. The data were processed and analyzed using Bruker XWINNMR software (Bruker Analytische Messtechnik, GmbH, version 2.7).

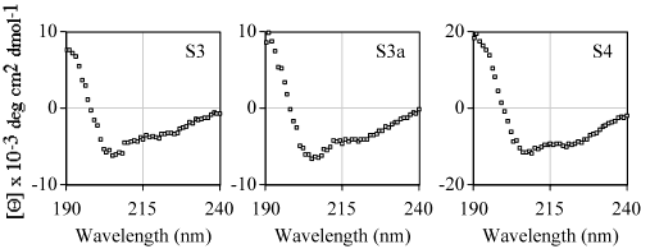

FIGURE 1: Far-UV circular dichroism spectra of dermaseptins S3, S3a, and S4. CD spectra were taken for 0.3 mM peptide samples (determined by UV using standard curves of known concentrations for each peptide) in a 20% trifluoroethanol/water mixture. CD data represent average values from three separate recordings.

Resonance assignment was done according to the sequential assignment methodology developed by Wüthrich (*37*) based on the TOCSY and NOESY spectra measured under identical experimental conditions. The distance restraints from the experimental data were calculated using AURELIA (Bruker) and calibrated according to the known distance of 2.66 Å between adjacent protons of the indole tryptophan ring. Data processing, calculations, and analyses were carried out on Silicon Graphics workstations (INDY R4000). The $^3J_{NH_\alpha}$ scalar couplings were calculated using a Lorentzian line fit for the line shapes of the relevant peaks in the TOCSY spectra (AURELIA).

The three-dimensional structures of the peptides were generated using XPLOR (*38*) (version 3.856). The structures were calculated from the NMR-derived restraints by first embedding the experimental data on peptide templates and then using distance geometry and restrained simulated annealing followed by restrained molecular dynamics and energy minimization. NOE ranges were within 1.1 Å above and 0.5 Å below the calculated distance to account for internal motion. The NOE energy was introduced as a square-well potential with a constant force constant of 50 kcal mol^{-1} Å^{-2}. Simulated annealing consisted of 3 fs steps (1500) at 1000 K and 1 fs steps (3000) during cooling to 300 K. Finally, the structures were minimized using conjugate gradient energy minimization for 4000 iterations. InsightII (Molecular Modeling System version 97.0, Molecular Simulations, Inc.) was used for analysis and presentation. Low-energy structures chosen for further analysis had no NOE violations above 0.5 Å, deviations from ideal bond lengths of less than 0.05 Å, and bond angle deviations from ideality of less than 5°. The PROCHECK (*39*) program was used to analyze the secondary structures of the calculated conformations.

RESULTS

To determine and compare the solution molecular organization of dermaseptin S3 and its amidated analogue, we performed both CD and NMR measurements.

CD Measurements. Preliminary indications of the molecular organization of the peptides in solution were obtained from CD measurements in water and TFE solutions. In water, both peptides displayed typical spectra of unordered structures (data not shown). However, in the less polar medium of 20% TFE, the CD spectra of both the native and amidated peptides displayed a clear shift toward ordered structure (Figure 1). Although the CD spectra showed a general curve similar to the canonical spectrum of an α-helical peptide, the native and amidated peptides exhibited minima at slightly lower wavelengths. No concentration dependence was observed in the range of 0.1−0.8 mM. Under the same conditions, dermaseptin S4 displayed a CD spectrum of a typical α-helix as characterized by double minima at 208 and 222 nm (*40*, *41*).

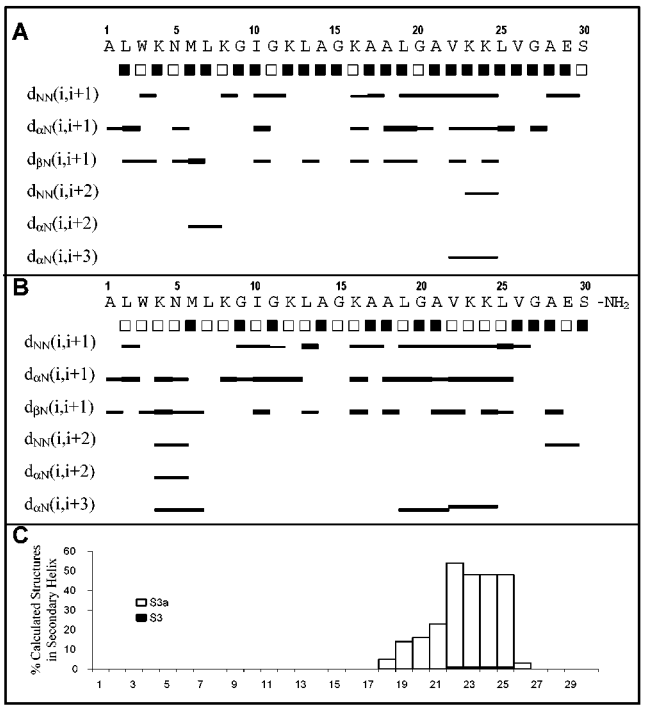

FIGURE 2: Summary of the NOE data and $^3J_{NH_\alpha}$ couplings above (■) and below (□) 4.6 Hz, together with NOE connectivities within dermaseptins (A) S3 and (B) S3a. (C) The percentage of accepted calculated conformations that exhibited an α-helix for S3 (filled columns) and S3a (empty columns).

NMR Measurements. The NMR NOESY spectrum of dermaseptin S3 in 20% (v/v) trifluoroethanol-d_3 in water generally showed a single set of sharp, well-resolved signals, indicating a monomeric state under experimental conditions (summarized in Figure 2). The $^3J_{NH_\alpha}$ coupling constants within the range of 5.0−8.9 Hz indicate fast averaging of different conformations in solution (Figure 2A at the top). The sequential NOE connectivity plot did not give any clear indication of a preferred conformation. Interproton distance restraints used in the structure calculations included 225 restraints, of which 179 were intraresidual, 58 sequential, and 18 medium-range. Of the 100 calculated conformations, 76 were accepted (see Materials and Methods for criteria) and used for further analysis. An ensemble of 35 low-energy conformations calculated for S3 and superimposed on their average structure has a backbone rmsd of 4.7 Å (SD = 0.6 Å). Although S3 shows no dominant conformation, the turn in the C-terminal region causes the peptide backbone to turn back on itself, yielding a calculated conformational space with an overall average length of 39 ± 5 Å.

Secondary structural elements along the peptide were identified by the PROCHECK program and were considered to be the dominant conformation in solution when present in at least half of the accepted calculated structures. PROCHECK identified a hydrogen-bonded turn at residues Lys23 and Lys24 with extensions to Val22 and through Val26. There were bends at Gly9, -15, -20, and -27 and

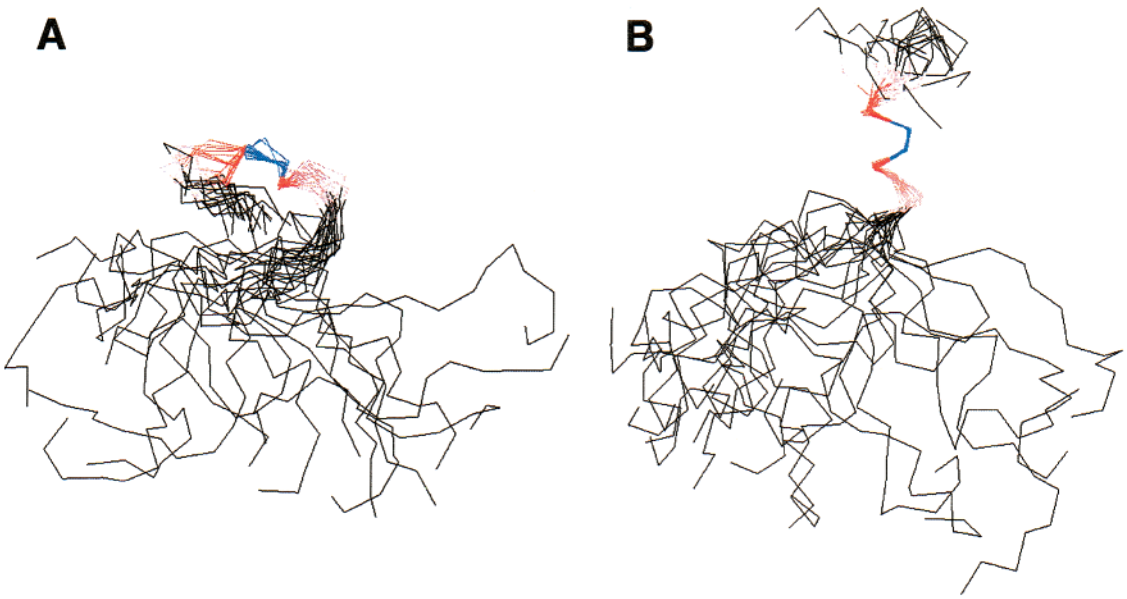

FIGURE 3: Ensembles of 20 low-energy accepted calculated conformations of dermaseptins (A) S3 and (B) S3a superimposed on residues 22−25 of the average calculated structure of each showing the amphipathic separation into hydrophilic (blue) and hydrophobic (red) residues in the region of residues 22−25.

Ala21. Figure 3A shows 20 low-energy peptide conformations superimposed over the identified turn at residues 22−25. The conformational space of S3 shows that the C-terminus region is compacted in upon itself (Figures 3A and 4). Only a negligible number of the structures exhibited a helix turn within these residues (Figure 2C).

The two-dimensional NOESY spectrum of the amidated analogue, dermaseptin S3a, also exhibited a discreet set of sharp, resolved signals. The $^3J_{NH_\alpha}$ coupling constants of the peptide are shown at the top of Figure 2B. The coupling constants are clearly lower on average than those of the nonamidated peptide, and there is a long patch between residues 22 and 25 with coupling constants below 4.6 Hz. The NOE pattern (Figure 2B) shows connectivities of types NN(i,i+1), αN(i,i+1), and αN(i,i+3), indicative of an α-helix in this region.

The NOESY spectrum of S3a gave 205 NOE distance restraints, of which 134 were intraresidual, 57 sequential, and 14 medium-range. Of the initial 100 refined structures, 79 passed the acceptance criteria. The calculated structures of S3a have an overall backbone rmsd of 3.58 Å (SD = 0.6 Å) when superimposed on their average structure. This is lower than the value of 4.7 Å (SD = 0.6 Å) found for native dermaseptin S3. PROCHECK analysis identified an α-helix between residues 22 and 25 of dermaseptin S3a (constituting 13% of the sequence of the peptide) with a backbone rmsd of 0.81 Å (SD = 0.07 Å) (Figure 3B). The conformational space described by the calculated structures of the amidated peptide is extended due to the helix at residues 22−25 and has an overall average length of 50 ± 5 Å. This is ∼30% more extended than the native peptide (Figure 4). Bends were also identified at residues Trp3, Ile10, Leu13, and Ala28.

When the calculated low-energy structures are superimposed over the region of the helix (residues 22−25, Figure 3), the pronounced difference in the structural organization of the more ordered S3a and S3 becomes clear. The C-terminal region of the peptide is extended by the α-helix as opposed to the turn present in dermaseptin S3 in this region that leads it to be gnarled and nonstructured. The two peptides, superimposed over residues 22−25, show the extension past residue 25 in dermaseptin S3a where the C-terminus in native S3 virtually turns back upon itself. Figure 3B emphasizes the amphipathic separation of hydrophilic residues K23 and K24 (in blue) from hydrophobic residues Leu22 and Val 25 (in red) due to the helical organization. Figure 4 clearly shows the difference in the length of the conformational space of each peptide.

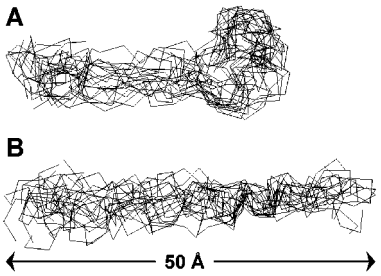

FIGURE 4: Ensembles of 20 low-energy accepted calculated conformations of dermaseptins (A) S3 and (B) S3a superimposed on their average structure showing the approximately 30% difference in the length spanned by the conformational space of each peptide.

DISCUSSION

Structural information regarding a system under study often gives important, if not essential, information that can be used to understand mechanisms of action and for tailored molecular design. NMR is increasingly being used to study antimicrobial peptides both qualitatively and structurally despite the inherent difficulty due to the flexibility of peptides 20−50 residues in length. The reported NMR-derived structures of many characterized antimicrobial peptides have rmsd values within the range from 0.4 Å to a few angstroms, indicating that they represent a dominant solution conformation. Despite their common wide-spectrum antimicrobial action, these peptides have been shown to have a range of conformations from ordered or partial α-helices (*42*−*45*) and

β-sheets (*46*−*48*) and mixtures of these (*49*) to only partially ordered (*50*) or mainly random conformations (*51*). As the availability of NMR data increases, structural studies of antimicrobial peptides comparing NMR results to CD results are being carried out. Many show a correlation between the results of both methods (*52*, *53*), while some do not (*54*).

The peptide structures can be sensitive to the medium that is used (*28*, *33*), making the choice of environment for structural studies critical. We chose to look at the peptide structure immediately prior to its interaction with the membrane, which we believe represents a crucial moment that leads to cell permeabilization. At that very moment, the peptide is still in an aqueous medium but is likely to be affected by the membrane environment. To mimic such an interface milieu, structural studies were performed in an aqueous medium somewhat more hydrophobic than water (i.e., 20% trifluoroethanol). Such a milieu is often used to investigate peptide structure (*33*, *44*, *45*).

CD measurements failed to distinguish between S3 and S3a structures and suggested that both peptides have a predominant α-helical structure. Although the extrema of the CD spectra were not identical to those of standard α-helix reference spectra, the curves themselves were similar in shape to standard curves and could easily be misinterpreted. Despite the CD indications of the presence of α-helical structure, NMR-derived structures showed no helical structure in native S3 and <15% α-helix in the amidated peptide even though the NMR studies were carried out in a 20% TFE/water solution, known to stabilize α-helical structure in compounds with a propensity for helix formation (*55*, *56*).

Compared with the native peptide, S3a has been shown to display increased potency over a broad range of pathogens, with a minimal inhibitory concentration (MIC) reduced by 2−10-fold, depending on the organism (*22*). Increased potency in amidated antimicrobial peptides is often attributed to the increased overall positive charge (*8*, *15*−*18*). In this case, however, amidation has done more than just modify the total charge. It has induced helix formation at the C-terminus or stabilized existing helical conformations. The numerous bends and turn identified in native S3 result in a compacted C-terminus and a reduction in the overall physical length of the conformational space occupied by the peptide. It is possible that this turn and the bends represent a nascent helix (*56*) in S3 in this region, and the amidation stabilizes this conformation relative to others present in solution. Overall, the native S3 and its amidated analogue, investigated under otherwise identical conditions, showed two major differences.

(i) The peptides differ significantly in their overall structures. S3a has an average helix content of 13% in its C-terminal region at residues 22−25 extending to positions 20 and 27. This region is also characterized by low *J* coupling values and NOE connectivities characteristic of helices. There are no regions in native S3 with any helical structure or reduction in *J* coupling (Figures 2 and 3). Since amphipathic organization is widely known to enhance antimicrobial activity, it is noteworthy that both S3 and S3a lack amphipathicity, although both peptides have potent and wide-spectrum antimicrobial activity. This discrepancy calls into question the importance of amphipathic organization during the initial step of peptide−membrane interaction. One might observe that the resulting helix loop in S3a did organize the side chains in this region of the peptide into a seemingly amphipathic division centered around K23 and K24 (Figure 3B). It is therefore possible that an amphipathic structure will fully develop upon further interaction with the membrane.

(ii) The overall physical lengths of the conformational space spanned by the two peptides differ significantly as a result of their structures. The helix at the C-terminus causes the amidated peptide to be approximately 30% longer than the native S3 (Figure 4). Truncation reduces peptide length and has often been shown to alter activity (*57*, *58*). In most instances, reduced length by truncation was associated with reduced potency (*20*, *22*, *28*, *33*), although truncation also alters important properties such as charge and hydrophobicity, along with their accompanying differences in activity. The difference in length shown here implicates physical length as a possible factor influencing activity without any alteration of the sequence itself, apart from amidation. At the beginning of its interaction with the target membrane, the amidated peptide presents a longer and more rigid structure than native dermaseptin S3. Together, both properties (i and ii) may account for the enhanced growth inhibition potency of the amidated peptide.

C-Terminally truncated derivatives of dermaseptin S3 still show a MIC of a similar order of magnitude as that of the full-length peptide (*22*), indicating that, at least against certain microorganisms, the C-terminal region does not participate in the cytolytic activity, as was shown for other members of the dermaseptin family (*20*, *28*). However, when the C-terminus is truncated, activity against other pathogens (e.g., *Streptomyces aureus* or *N. brasiliensis*) drops drastically, indicating the role of the C-terminal region in selectivity. Therefore, the enhanced potency and selectivity observed in S3a may be as a result of the structural changes in the C-terminal region, induced by amidation, and must be considered when carboxyamidation is being evaluated for any purpose.

With respect to the N-terminal region, S3 displays a molecular organization strikingly different from that of S4, despite their high level of homology in primary structure (Table 1). Under identical experimental conditions, the N-terminal domain of S4 displayed a high tendency to fold into a nearly perfect α-helical and amphipathic structure (*33*) The fact that S3 was devoid of such a tendency even though it displayed a higher antibacterial potency (*22*) especially against clinical isolates (*31*) raises questions about the full importance of helicity and amphipathicity in the interaction of antibacterial peptides with target cells. Possibly, high flexibility prevents aggregation in solution that, in turn, hampers antibacterial activity (*29*, *33*). In this respect, our results are in accord with previous studies, although based on FTIR and not NMR, that linked higher antibacterial potency with less structured diastereoisomeric peptides (*59*).

In conclusion, native dermaseptin S3 was found to have a flexible structure under the experimental conditions. We show that C-terminus amidation induces α-helix formation and/or stabilizes the peptide in this conformation, as this was the only parameter that was altered. The enhanced growth inhibition activity may thus be ascribed to the increase in positive charge, the increase in helix content, the increase in length and rigidity, or any subset of the above, but the structural changes in the peptide upon amidation cannot be

discounted. Further work will be done to assess each of these parameters independently.

ACKNOWLEDGMENT

The expert assistance of Leonid Gudaikov in providing the CD spectra is gratefully acknowledged.

SUPPORTING INFORMATION AVAILABLE

A table of chemical shifts of S3 and S3a dermaseptin peptides together with a list of NOE constraints used for the structure calculation. This material is available free of charge via the Internet at http://pubs.acs.org.

REFERENCES

1. García-Olmendo, F., Carmona, M. J., Lopez-Fando, J. J., Fernandez, J. A., Castagnaro, A., Molina, A., Hernandez-Lucas, C., and Carbonero, P. (1992) in *Genes Involved in Plant Defense* (Boller, T., and Meins, F., Eds.) pp 283−302, Springer-Verlag, New York.
2. Andreu, D., and Rivas, L. (1998) *Biopolymers 47*, 415−433.
3. Nicolas, P., and Mor, A. (1995) *Annu. Rev. Microbiol. 49*, 277−304.
4. Hancock, R. E. W. (1997) *Lancet 349*, 418−422.
5. Boman, H. (1995) *Annu. Rev. Immunol. 13*, 61−92.
6. Hernandez, C., Mor, A., Dagger, F., Nicolas, P., Hernandez, A., Benedetti, E. L., and Dunia, I. (1992) *Eur. J. Cell Biol. 59*, 414−424.
7. Strahilevitz, J., Mor, A., Nicolas, P., and Shai, Y. (1994) *Biochemistry 33*, 10951−10960.
8. Pouny, Y., Rapaport, D., Mor, A., Nicolas, P., and Shai, Y. (1992) *Biochemistry 31*, 12416−12423.
9. Fox, R. O., and Richards, F. M. (1982) *Nature 300*, 325−330.
10. Schwarz, G., Gerke, H., Rizzo, V., and Stankowski, S. (1987) *Biophys. J. 52*, 658−692.
11. Shai, Y. (1994) *Toxicology 87*, 109−129.
12. Epand, M. E., Shai, Y., Segrest, J. P., and Anantharamaiah, G. M. (1995) *Biopolymers 37*, 319−338.
13. Shai, Y. (1995) *Trends Biochem. Sci. 20*, 460−464.
14. Bechinger, B., Zasloff, M., and Opella, S. J. (1992) *Biophys. J. 62*, 12−14.
15. Cociancich, S., Ghazi, A., Hetru, C., Hoffmann, J. A., and Letellier, L. (1993) *J. Biol. Chem. 268*, 19239−19245.
16. Ludtke, S., He, K., and Huang, H. (1995) *Biochemistry 34*, 16764−16769.
17. Steiner, H., Andreu, D., and Merrifield, R. B. (1988) *Biochim. Biophys. Acta 939*, 260−266.
18. Genaro, R., Skerlavaj, B., and Romeo, R. (1989) *Infect. Immun. 57*, 3142−3146.
19. Matsuzaki, K., Yoneyama, S., Fujii, N., Miyajima, K., Yamada, K., Kirino, Y., and Anzai, K. (1997) *Biochemistry 36*, 9799−9806.
20. Feder, R., Dagan, A., and Mor, A. (2000) *J. Biol. Chem. 275*, 4230−4238.
21. Oren, Z., Hong, J., and Shai, Y. (1997) *J. Biol. Chem. 272*, 14643−14649.
22. Mor, A., Hani, K., and Nicolas, P. (1994) *J. Biol. Chem. 269*, 31635−31641.
23. Dykes, G. A., Aimoto, S., and Hastings, J. W. (1998) *Biochem. Biophys. Res. Commun. 248*, 268−272.
24. Wieprecht, T., Dathe, M., Beyermann, M., Krause, E., Maloy, W. L., MacDonald, D. L., and Bienert, M. (1997) *Biochemistry 36*, 6124−6132.
25. Chen, C., Seow, K. T., Guo, K., Yaw, L. P., and Lin, S.-C. (1999) *J. Biol. Chem. 274*, 19799−19806.
26. Mor, A., and Nicolas, P. (1994) *Eur. J. Biochem. 219*, 145−154.
27. Charpentier, S., Amiche, M., Mester, Y., Vouille, V., Le Caer, J. P., Nicolas, P., and Delfour, A. (1998) *J. Biol. Chem. 273*, 14690−14696.
28. Mor, A., and Nicolas, P. (1994) *J. Biol. Chem. 269*, 1934−1939.
29. Ghosh, J. K., Shaool, D., Guillaud, P., Ciceron, L., Mazier, D., Kustanovich, I., Shai, Y., and Mor, A. (1997) *J. Biol. Chem. 272*, 31609−31616.
30. Oren, Z., and Shai, Y. (1998) *Biopolymers 47*, 451−463.
31. Jouenne, T., Mor, A., Bonato, H., and Junter, G. A. (1998) *J. Antimicrob. Chemother. 42*, 87−90.
32. Coot, P. J., Holyoak, C. D., Bracey, D., Ferdinando, D. P., and Pearce, J. A. (1998) *Antimicrob. Agents Chemother. 42*, 2160−2170.
33. Kustanovich, I., Shalev, D. E., Mikhlin, M., Gudaikov, L., and Mor, A. (2002) *J. Biol. Chem. 277*, 16941−16951.
34. Bax, A., and Davis, D. G. (1985) *J. Magn. Reson. 65*, 355−360.
35. Kumar, A., Ernst, R. R., and Wüthrich, K. (1980) *Biochem. Biophys. Res. Commun. 95*, 1−6.
36. Macura, S., and Ernst, R. R. (1980) *Mol. Phys. 41*, 95−117.
37. Wüthrich, K. (1986) *NMR of Proteins and Nucleic Acids*, John Wiley & Sons, New York.
38. Nilges, M., Kuszewski, J., and Brunger, A. T. (1991) in *Computational Aspects of the Study of Biological Macromolecules by NMR* (Hoch, J. C., Ed.) pp 451−455, Plenum Press, New York.
39. Laskowski, R. A., Rullmann, J. A., MacArthur, M. W., Kaptein, R., and Thornton, J. M. (1996) *J. Biomol. NMR 8*, 477−486.
40. Greenfield, N., and Fasman, G. D. (1969) *Biochemistry 8*, 4109.
41. Yang, J. T., Wu, C.-S. C., and Martinez, H. M. (1986) *Methods Enzymol. 130*, 208−269.
42. Wong, H., Bowie, J. H., and Carver, J. A. (1997) *Eur. J. Biochem. 247*, 545−557.
43. Yi, G. S., Park, C. B., Kim, S. C., and Cheong, C. (1996) *FEBS Lett. 398*, 87−90.
44. Suh, J. Y., Lee, K. H., Chi, S. W., Hong, S. Y., Choi, B. W., Moom, H. M., and Choi, B. S. (1996) *FEBS Lett. 392*, 309−312.
45. Marion, D., Zasloff, M., and Bax, A. (1988) *FEBS Lett. 227*, 21−26.
46. Aumelas, A., Mangoni, M., Roumestand, C., Chiche, L., Despaus, E., Grassy, G., Calas, B., and Chavanieu, A. (1996) *Eur. J. Biochem. 237*, 575−583.
47. Kawano, K., Yoneya, T., Miyata, T., Yoshikawa, K., Tokunaga, F., Terada, Y., and Iwanaga, S. (1990) *J. Biol. Chem. 265*, 15365−15367.
48. Bach, A. C., II, Selsted, M. E., and Pardi, A. (1987) *Biochemistry 26*, 4389−4397.
49. Martins, J. C., Maes, D., Loris, R., Pepermans, H. A., Wyns, L., Willem, R., and Verheyden, P. (1996) *J. Mol. Biol. 258*, 322−333.
50. Patel, S. U., Osborn, R., Rees, S., and Thorton, J. M. (1998) *Biochemistry 37*, 983−990.
51. Vignal, E., Chavanieu, A., Roch, P., Chiche, L., Grassy, G., Calas, B., and Aumelas, A. (1999) *J. Biochem. 253*, 221−228.
52. Clore, G. M., Martin, S. R., and Gronenborn, A. M. (1986) *J. Mol. Biol. 191*, 553−561.
53. Liu, A., Riek, R., Zahn, R., Hornenmann, S., Glockshuber, R., and Wüthrich, K. (1999) *Biopolymers 51*, 145−152.
54. Ladokhin, A. S., Selsted, M. E., and White, S. H. (1999) *Biochemistry 38*, 12313−12319.
55. Segawa, S., Fukuno, T., Fujiwara, K., and Noda, Y. (1991) *Biopolymers 31*, 497−509.
56. Dyson, H. J., Rance, M., Houghten, R. A., Wright, P. E., and Lerner, R. A. (1988) *J. Mol. Biol. 201*, 201−217.
57. Muraki, M., Morii, H., and Harata, K. (2000) *Protein Eng. 13*, 385−389.
58. Park, C. B., Yi, K. S., Matsuzaki, K., Kim, M. S., and Kim, S. C. (2000) *Proc. Natl. Acad. Sci. U.S.A. 97*, 8245−8250.
59. Oren, Z., and Shai, Y. (1997) *J. Biol. Chem. 272*, 14643−14649.

BI016013M